RSC Advances

PAPER

View Article Online
View Journal | View Issue

Cite this: *RSC Adv.*, 2023, **13**, 7614

Waste-biomass-derived activated carbon supported Co–Cu–P nanocatalysts for hydrolytic dehydrogenation of ammonia borane†

Lei Wei, * Yanhong Lu, Ruixuan Lu and Yuxin Cui

Received 13th January 2023
Accepted 26th February 2023

DOI: 10.1039/d3ra00247k

rsc.li/rsc-advances

Hydrolytic dehydrogenation of ammonia borane is a significant and promising approach for on-site hydrogen production at ambient conditions, and developing highly efficient and low-cost catalysts has attracted considerable attention. Herein, waste-biomass-derived activated carbon (AC) was prepared by hydrothermal carbonization and alkali-assisted activation, and non-precious bimetal phosphides (Co–Cu–P) nanocatalysts with a series of different Co/Cu ratios were synthesized on the AC surface through *in situ* phosphidation method. Owing to the synergetic effects, the optimal $Co_{0.8}Cu_{0.2}P$/AC presents an outstanding turnover frequency of 26.5 min^{-1} (25 °C), which is much higher than that of many reported catalysts. The reaction activation energy was measured to be 34.6 kJ mol^{-1}. Benefiting from the ferromagnetic nature of the phosphides, the $Co_{0.8}Cu_{0.2}P$/AC can be magnetically separated and reused again. After recycling six times, the catalyst still retains 72% of the initial activity, thus indicating great potential for practical applications.

Introduction

With the rapid utilization of hydrogen energy, ammonia borane (NH_3BH_3, AB) has emerged as one of the most promising chemical hydrides for hydrogen storage.[1,2] In theory, AB presents a hydrogen content of up to 19.6 wt%, which is much higher than that of other hydrides such as sodium borohydride, formic acid, hydrazine hydrate, *etc.*[3] According to eqn (1), hydrolytic dehydrogenation of AB in the presence of suitable catalysts can release three equivalent hydrogens. For the practical applications in hydrogen production, the investigation of catalysts is of critical importance.[4,5]

$$NH_3BH_3 + 2H_2O \xrightarrow{\text{Catalyst}} NH_4BO_2 + 3H_2\uparrow \quad (1)$$

A series of recent studies have indicated that low-cost and efficient catalysts are exceedingly desired for AB hydrolysis. Because of the drawbacks involving low reserves and high cost, noble metal catalysts like Ru, Pt, Rh cannot satisfy the requirements of large-scale industrial utilization. Therefore, considerable attention has been paid to non-precious metal catalysts, especially transition metal phosphides such as CoP and Ni_2P.[6,7] However, the catalytic activity of the monometal phosphides needs to be further improved to achieve high efficiency of AB dehydrogenation. To this end, bimetal phosphides have been suggested as highly efficient catalysts for hydrogen generation from AB hydrolysis due to the synergetic effect. For instance, Yang *et al.* prepared Ni–Fe–P catalysts on Ni foam by electroless plating, and the Ni–Fe–P/Ni presented much higher activity than that of Ni–P/Ni and Fe–P/Ni.[8] Additionally, Zhou *et al.* found that boron nitride supported $Ni_{0.8}Co_{1.2}P$ nanoparticles (NPs) exhibited optimal catalytic performance for AB hydrolysis thanks to the synergistic effect.[9]

To prevent the aggregation of nanocatalysts, the use of porous supports like carbon-based material, zeolite, and metal–organic frameworks has been confirmed to be feasible. Among various supports, activated carbon (AC) is extremely popular and possesses many advantages including low cost, excellent porosity, high specific surface area, and stable physicochemical property. Currently, the cost-effective AC derived from waste biomass has attracted increasing interest. As reported in recent literature, there are many kinds of biomass used for AC production, including cattail, cotton, walnut shell, shaddock endothelium, pinecone shell, corn straw, and so on.[10–15]

In our present work, waste ginkgo leaves were collected for the preparation of AC *via* traditional hydrothermal carbonization and alkali-assisted activation. *In situ* phosphidation method was conducted for the synthesis of Co–Cu–P nanocatalysts immobilized on the waste-biomass-derived AC, and the Co/Cu ratio was optimized to realize the highest catalytic activity for AB hydrolysis. To our knowledge, there have been no similar research reports so far. As expected, due to the synergetic effect and support effect, the optimum $Co_{0.8}Cu_{0.2}P$/AC presents an extremely high activity for catalytic hydrolysis of

College of Chemistry and Materials Science, Langfang Normal University, Langfang 065000, P. R. China. E-mail: weilei@lfnu.edu.cn

† Electronic supplementary information (ESI) available: ICP results of the prepared catalysts, and XPS spectrum of B 1s of the reused catalyst. See DOI: https://doi.org/10.1039/d3ra00247k

AB, compared with many cobalt-based catalysts reported in literature. In addition, hydrolytic kinetics and catalyst reusability were also investigated in detail.

Experimental

Chemicals

All chemicals including cobalt nitrate hexahydrate ($Co(NO_3)_2 \cdot 6H_2O$, AR), copper nitrate trihydrate ($Cu(NO_3)_2 \cdot 3H_2O$, AR), sodium hypophosphite monohydrate ($NaH_2PO_2 \cdot H_2O$, AR), potassium hydroxide (KOH, AR), hydrochloric acid (HCl, 37%), and ammonia borane (NH_3BH_3, 97%) were purchased from Shanghai Aladdin Bio-Chem Technology Co., Ltd, China. Deionized water was used throughout this experiment.

Preparation of AC

For the preparation of biomass-derived AC, detailed procedures involving pre-treatment, hydrothermal carbonization, and alkali-assisted activation were described in our previous work.[15] The collected ginkgo leaves were completely dried in an electric oven at 90 °C and then shattered. To obtain fine powder, sieving operation was done with a 100 mesh sieve. In a typical run, 4.00 g of the fine powder was dispersed in 60 mL deionized water by vigorous stirring and then transferred to a 100 mL Teflon-lined autoclave, followed by heating at 180 °C for 12 h. After cooling to room temperature, the hydrothermal product was filtered, washed, and completely dried. Next, 2.00 g of the hydrothermal product was uniformly mixed with 1.00 g of KOH and then heated at 700 °C for 1 h under argon atmosphere. After natural cooling, the activated product was successively washed with diluted HCl and deionized water until the pH value was constant to be 7.0. The biomass-derived AC was finally achieved after conventional filtration and drying.

Synthesis of Co–Cu–P/AC

Metal phosphide was synthesized by *in situ* phosphidation method, and the detailed installation and procedure were introduced in our recent work.[16] At first, 0.20 g of the obtained AC was added into 15 mL precursor solution containing $Co(NO_3)_2$ and/or $Cu(NO_3)_2$. The molar ratios of Co to Cu were given to be 1.0 : 0, 0.8 : 0.2, 0.6 : 0.4, 0.4 : 0.6, 0.2 : 0.8, and 0 : 1.0, respectively, while the molar mass of Co and Cu was fixed to be 0.34 mmol. After moderate stirring at room temperature for 1 h, water in the solid–liquid system was completely evaporated, and the inorganic salts would be uniformly deposited on the AC surface. The phosphating process was performed at 300 °C for 1.5 h, and 0.15 g of the $NaH_2PO_2 \cdot H_2O$ was used for each run. Finally, a series of $Co_xCu_{1-x}P$/AC catalysts ($x = 1.0$, 0.8, 0.6, 0.4, 0.2, 0) were achieved. The contents of Co and Cu in each sample were determined by ICP and shown in Table S1.†

Characterization

The micromorphology and element distribution were analysed by a field-emission scanning electron microscope (FE-SEM, Hitachi S-4800) and a transmission electron microscope (TEM, FEI Tecnai G2 F20) coupled with OXFORD MAX-80 energy dispersive X-ray system. The crystalline structure of solid samples was examined on a Rigaku D/Max-2500 X-ray diffractometer (XRD) with Cu Kα radiation. X-ray photoelectron spectroscopy (XPS) characterization was conducted on a Thermo ESCALAB 250Xi spectrometer. The specific surface area and pore size distribution were typically measured by means of N_2 adsorption/desorption isotherms. Raman spectrum was obtained with a Renishaw Raman spectrometer using laser excitation at 532 nm. The major parameters of magnetic material were determined on a vibration sample magnetometer (VSM, Quantum Design PPMT).

Catalytic activity measurement

Catalytic activity of the prepared $Co_xCu_{1-x}P$/AC for AB hydrolysis was measured as follows. The volume of generated hydrogen was monitored by the water-displacement method using a testing setup described elsewhere.[17] Typically, 10 mg of the catalyst was dispersed in 5.0 mL aqueous solution containing 1.0 mmol AB, and the reaction temperature was kept at 25 °C by a water bath. Turnover frequency (TOF) was calculated according to eqn (2).

$$\mathrm{TOF} = \frac{n_{H_2}}{(n_{Co} + n_{Cu})t} \quad (2)$$

where n_{H_2} is the total molar mass of the generated hydrogen, t is the reaction time for complete hydrolysis of AB, and n_{Co} and n_{Cu} represent the molar mass of Co and Cu elements in the catalyst, respectively.

Kinetics of AB hydrolysis

The optimum catalyst with the highest TOF was chosen for further investigation. A series of hydrolysis reaction over the optimum catalyst was done to determine the reaction kinetics. First, the catalyst amount and temperature were kept at 10 mg and 25 °C, and the AB concentration was varied at 0.10, 0.20, 0.30, and 0.40 mol L^{-1}, respectively. Second, the AB concentration and reaction temperature were maintained at 0.20 mol L^{-1} and 25 °C, respectively, whereas the catalyst amount was changed from 5 to 20 mg. Finally, the reaction was performed at different temperature in the range of 20–35 °C, and the AB concentration and catalyst amount were fixed at 0.20 mol L^{-1} and 10 mg, respectively.

Reusability testing

To assess the reusability of the optimum catalyst for AB hydrolysis, one dosage of the catalyst (10 mg) was repeatedly used six times, while maintaining the AB concentrate and reaction temperature at 0.20 mol L^{-1} and 25 °C, respectively. After each run, the used catalyst was isolated and washed before reusing again. In addition, the reused catalyst was finally gathered for chemical composition analysis.

Results and discussion

Characterization of the AC

In our experiment, the as-prepared AC derived from waste biomass was studied in advance. The SEM image in Fig. 1(a)

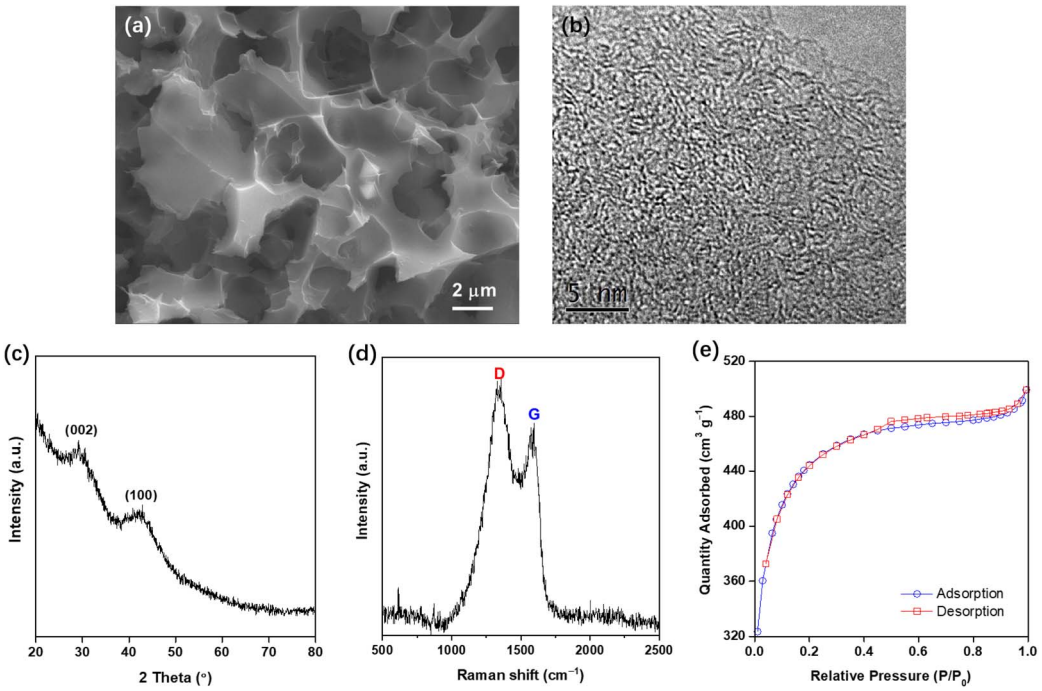

Fig. 1 Characterization results of the as-prepared AC: (a) FE-SEM and (b) high-resolution TEM images, (c) XRD pattern, (d) Raman spectrum, and (e) N_2 adsorption/desorption isotherms.

demonstrates the AC morphology, and the carbonized surface is representative and in good accord with literature results.[10,14,15] High-resolution TEM image in Fig. 1(b) clearly shows the porous nature.[15] According to the XRD pattern in Fig. 1(c), two weak and broad diffraction peaks around 29° and 42° correspond to the (002) and (100) planes of the graphite carbon, respectively, implying low ordering.[10–15]

Fig. 1(d) shows the Raman spectrum of the obtained AC, and the typical D- and G-bands located at 1340 and 1590 cm^{-1} can be assigned to the disordered carbon crystallites and crystalline graphite, respectively. To evaluate the structural defects and the degree of graphitization, the intensity ratio of the D- and G-bands (I_D/I_G) was calculated to be 1.26, indicating carbon in the obtained AC is mainly present in the form of disordered carbon.[10,11,15,18,19] Fig. 1(e) exhibits the N_2 adsorption/desorption isotherms, and specific surface area of the AC was calculated to be 1590 $m^2\ g^{-1}$ according to the well-known BET equation, which is comparable to some commercial AC material such as YP-50.[15] Additionally, average pore size of the prepared AC was measured to be 2.3 nm by the BJH model, thus indicating the mesoporous feature. In summary, all the evidence above confirms the successful synthesis of biomass-derived AC in this experiment.

Optimizing of the Co/Cu ratio

Lots of studies have demonstrated that high activity of the bimetal catalysts can be attributed to the synergistic effect, and the ratio of different metal elements significantly influences the catalytic activity.[8,9,20,21] Density functional theory (DFT) was applied by Zhou *et al.* to investigate the synergistic effect of NiCoP/h-BN for catalytic hydrolysis of AB.[9] And they found that bimetal phosphide can effectively boost the adsorption capacity of H radical and decrease the adsorption capacity of H_2 over catalyst surface, which benefit to the hydrogen generation and releasing.

Herein, the biomass-derived AC supported Co–Cu–P nanocatalysts with varied Co/Cu ratios were evaluated for AB hydrolysis. As shown in Fig. 2, the highest H_2 generation rate is achieved when using the $Co_{0.8}Cu_{0.2}P$/AC, indicating that the $Co_{0.8}Cu_{0.2}P$/AC possesses the best catalytic activity among all the prepared samples. As expected, the optimum bimetal phosphide catalyst is more active than monometal phosphides (*i.e.*, CoP/AC, CuP/AC). TOF of AB hydrolysis over the

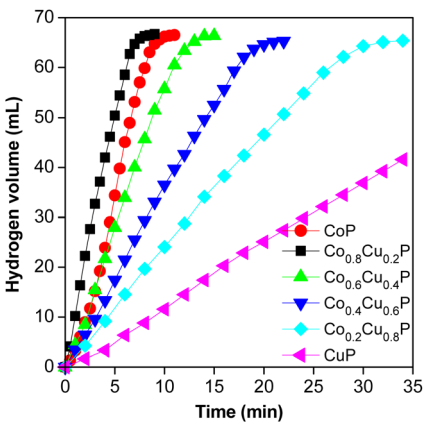

Fig. 2 Hydrogen evolution from AB hydrolysis using different catalysts.

Table 1 A comparison of the prepared $Co_{0.8}Cu_{0.2}P$/AC with similar catalysts in literature

Catalysts	TOF (min^{-1}) at 25 °C	Reference
$CuCo_2O_4$/Ti	32.8	22
$Co_{0.51}Cu_{0.49}$/C	28.7	23
CoCu@MIL-101	19.6	24
CoNi/graphene	16.4	25
CoB alloy	14.7	26
Co/graphene	13.8	27
PEI–Co	12.5	28
Cu@CoNi	15.5	29
P(VPA)–Co	7.7	30
Cu/Co_3O_4	7.0	31
Co/hydroxyapatite	5.8	32
$Co_{0.8}Cu_{0.2}P$/AC	26.5	This work

$Co_{0.8}Cu_{0.2}P$/AC was measured to be 26.5 min^{-1} at 25 °C, and the catalytic activity is much higher than that of many reported catalysts, as listed in Table 1.

Characterization of the $Co_{0.8}Cu_{0.2}P$/AC

Fig. 3(a)–(c) display the XRD patterns of the prepared CoP/AC, CuP/AC, and $Co_{0.8}Cu_{0.2}P$/AC, respectively. Remarkable diffraction peaks imply that the metal phosphides have good crystallinity. Compared with the XRD pattern of CoP/AC, due to the Cu incorporation in CoP, the peak at 26.5° shifts to 26.7°, and some extra peaks appear in the range of 15–25° (see Fig. 3(c)).[33] High-resolution XPS spectra of Co 2p, Cu 2p and P 2p showing the peak resolving and fitting for elements in the $Co_{0.8}Cu_{0.2}P$ are exhibited in Fig. 3(d)–(f). In Fig. 3(d), the peaks at 781.8 and 797.9 eV correspond to Co $2p_{3/2}$ and $2p_{1/2}$, respectively, while two board peaks at 786.1 and 803.1 eV are the satellite peaks of Co 2p.[24,25,29,34] In Fig. 3(e), the peaks at 932.4 and 952.5 eV can be assigned to Cu $2p_{3/2}$ and $2p_{1/2}$, respectively, and other peaks are associated with copper in copper oxide probably due to the inevitable superficial oxidation.[23,24,35] As shown in Fig. 3(f), two peaks located at 123.2 and 134.1 eV are recorded, which can be credited to the elemental P in metal phosphides and oxidized P species, respectively.[36,37]

According to TEM image in Fig. 4(a), it is clearly seen that the $Co_{0.8}Cu_{0.2}P$ NPs are loaded on the AC surface, and there are some inevitable aggregation happened in local surface. Such problem can be effectively solved by optimizing the loading amount of catalyst. As evidenced by EDS-mapping in Fig. 4(b), the green, red, and yellow dots stand for Co, Cu and P elements, respectively, confirming uniform distribution of the NPs all over the AC surface. By means of statistical analysis, particle size distribution of the $Co_{0.8}Cu_{0.2}P$ NPs was described in Fig. 4(c), and the average particle size was calculated to be 13.7 nm. High-resolution TEM images in Fig. 4(d) and (e) show obvious lattice fringes with a spacing of 0.186 nm analysed by Digital Micrograph software, which should be indexed to the (110) lattice plane. In addition, the result of selected area electron diffraction (SAED) pattern demonstrates the monocrystal nature of the obtained $Co_{0.8}Cu_{0.2}P$. Consequently, all the results mentioned above confirm the successful synthesis of $Co_{0.8}Cu_{0.2}P$ NPs on the biomass-derived AC.

Hydrogen generation measurement and kinetics analysis

Herein, we investigated the influence of AB concentration, catalyst amount, and reaction temperature on hydrogen evolution over the prepared $Co_{0.8}Cu_{0.2}P$/AC. Fig. 5(a) and (b) shows

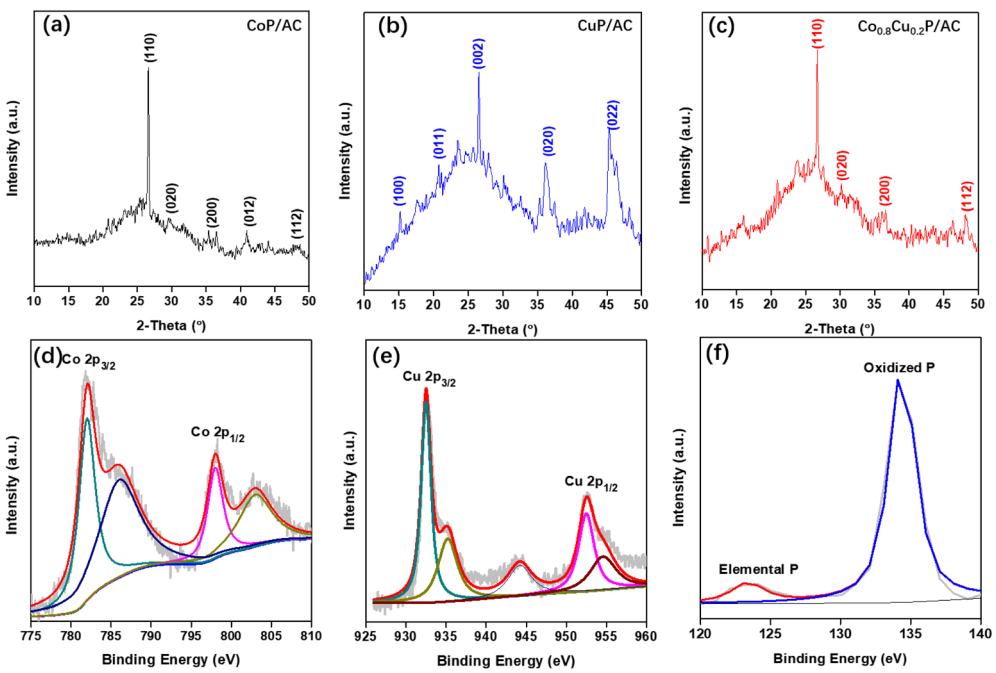

Fig. 3 XRD patterns of the prepared (a) CoP/AC, (b) CuP/AC and (c) $Co_{0.8}Cu_{0.2}P$/AC, respectively; high-resolution XPS spectra of (d) Co 2p, (e) Cu 2p and (f) P 2p of the $Co_{0.8}Cu_{0.2}P$, respectively.

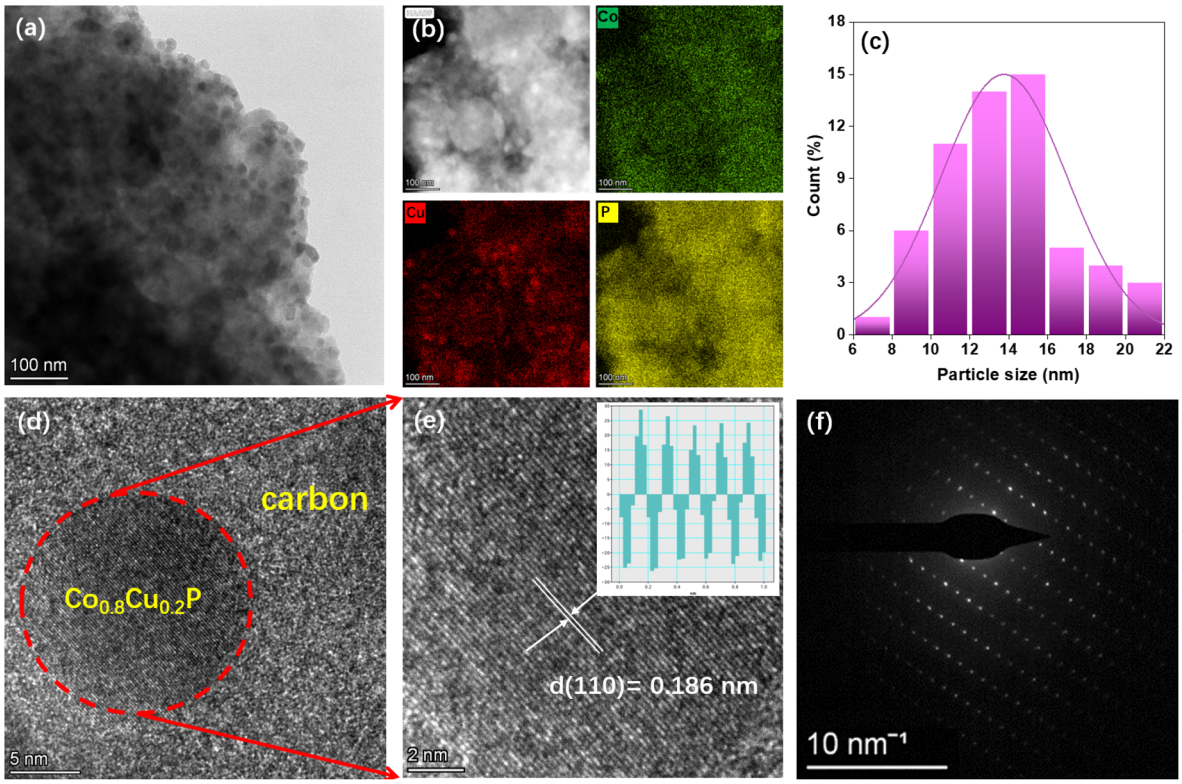

Fig. 4 (a) TEM image and (b) EDS mapping of the resulting $Co_{0.8}Cu_{0.2}P$/AC; (c) particle size distribution of the $Co_{0.8}Cu_{0.2}P$ NPs on the AC surface; (d and e) high-resolution TEM images (inset, spacing of crystal lattice) and (f) SAED image of the $Co_{0.8}Cu_{0.2}P$.

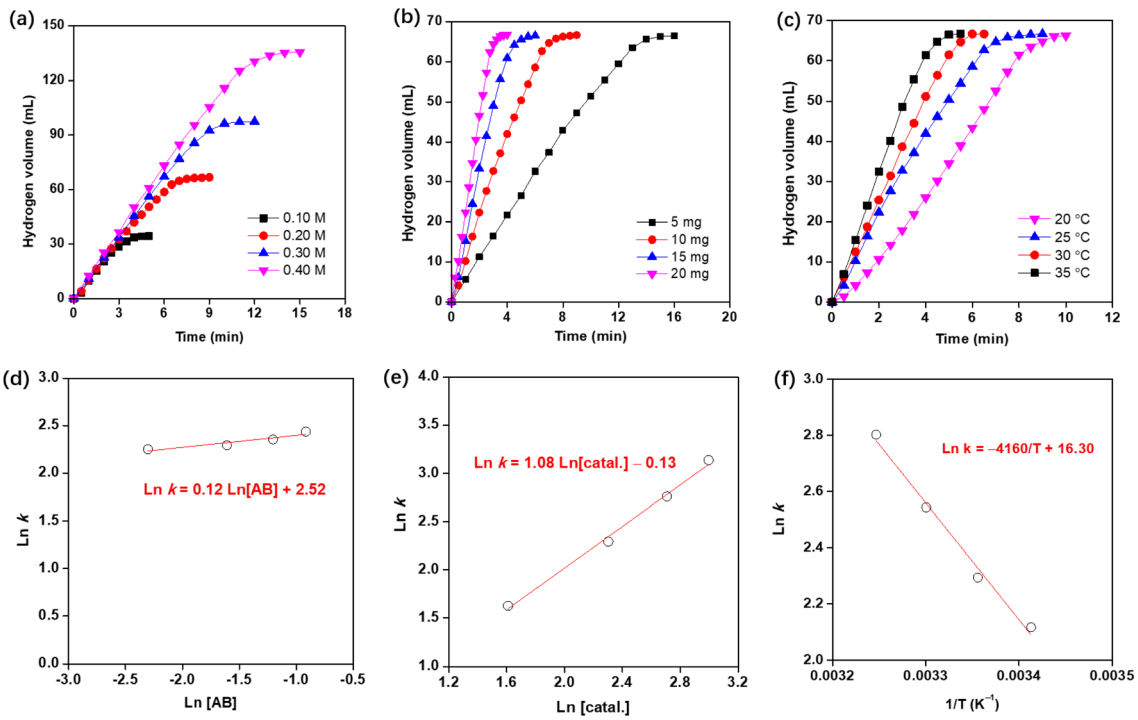

Fig. 5 Plots of reaction time *versus* volume of hydrogen generated from AB hydrolysis catalysed by the $Co_{0.8}Cu_{0.2}P$/AC under different (a) AB concentration, (b) catalyst amount and (c) reaction temperature. (d and e) Logarithmic plots of hydrogen generation rate (k) *versus* AB concentration and catalyst concentration, respectively. (f) Arrhenius plot of ln k *versus* 1/T.

the graphs of the volume of generated hydrogen *versus* time under varied AB concentration and catalyst amount, respectively. As can be seen in Fig. 5(a), the hydrogen generation rates are almost constant under varied AB concentrations. In Fig. 5(b), increasing the catalyst amount can greatly boost the hydrogen evolution from AB hydrolysis. Furthermore, the total generated hydrogen was nearly 3-fold of the used AB in mole, suggesting the complete dehydrogenation of AB. In most cases, it is quite normal that increasing temperature can lead to the improvement of hydrogen evolution, as shown in Fig. 5(c).[22–32]

Fig. 5(d) gives a straight line with a slope of 0.12, thus suggesting the catalytic hydrolysis of AB is zero-order with respect to the AB concentration. In Fig. 5(e), the slope of 1.08 of ln k and ln[catal.] indicates that AB hydrolysis over the $Co_{0.8}Cu_{0.2}P$/AC involves a first-order relative to catalyst concentration. In Fig. 5(f), we plot ln k *versus* $1/T$ based on the Arrhenius equation (eqn (3)).

$$\ln k = -(E_a/RT) + \ln A \quad (3)$$

The activation energy of AB hydrolysis catalyzed by the $Co_{0.8}Cu_{0.2}P$/AC is calculated to be 34.6 kJ mol^{-1}, which is much lower than many reported results such as $Co_{0.51}Cu_{0.49}$/C (51.9 kJ mol^{-1}),[23] Co/CTF (42.7 kJ mol^{-1}),[38] $Cu_{0.8}Co_{0.2}O$/GO (45.5 kJ mol^{-1}),[39] NiCoP/BN (40.3 kJ mol^{-1}),[9] and $Co_{0.79}B_{0.15}P_{0.06}$ (39.4 kJ mol^{-1}).[40]

Magnetic property and reusability

Recycling of the heterogeneous catalysts are frequently required in practical applications. As suggested in literature, magnetic catalysts endow easy separation with a magnet and reusing again.[25,29,41,42] Thus, magnetism analysis of the prepared $Co_{0.8}Cu_{0.2}P$/AC was performed on VSM in a range from −20 000 Oe to 20 000 Oe at room temperature, and the magnetic hysteresis loop is shown in Fig. 6. After calculation, the saturation magnetization is approximate to 9.8 emu g^{-1}, while remnant magnetization and coercivity were found to be 0.6 emu g^{-1} and 120 Oe, respectively. According to the photograph inset in Fig. 6, it is well illustrated that the $Co_{0.8}Cu_{0.2}P$/AC can be conveniently separated by an external magnet, further clarifying the ferromagnetic feature of the metal phosphide.

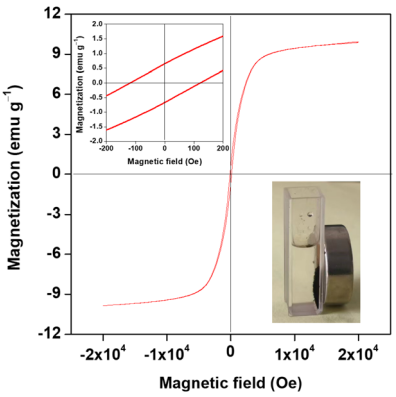

Fig. 6 Magnetic hysteresis loop of the prepared $Co_{0.8}Cu_{0.2}P$/AC (inset, optical photograph).

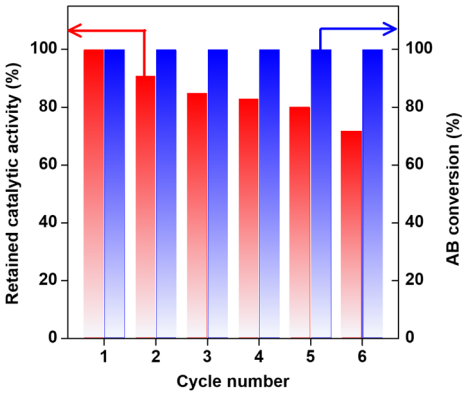

Fig. 7 Retained catalytic activity of the $Co_{0.8}Cu_{0.2}P$/AC and AB conversion in successive runs for AB hydrolysis.

We investigated the recycling stability of the prepared $Co_{0.8}Cu_{0.2}P$/AC for AB hydrolysis, and detailed results are shown in Fig. 7. It can be observed that the catalytic activity gradually decreases in successive cycles, but the AB conversion is always constant to be 100%. After recycling six times, the catalyst still retains 72% of the initial activity, thus implying the $Co_{0.8}Cu_{0.2}P$/AC possess relatively stable performance and great potential in practical applications. As reported in literature, activity degradation of the catalysts in successive hydrolysis of AB is a common phenomenon, and the primary reason is often ascribed to deposition of metaborate over the catalyst surface.[20,22,25,29,33,35,43,44] To verify such conjecture, XPS analysis toward the reused catalyst was performed. As shown in Fig. S1,† the peak of B 1s can be clearly observed at 192.7 eV, indicating the existence of metaborate on the catalyst surface.

Conclusions

In summary, non-precious bimetal phosphide (Co–Cu–P) as an efficient catalyst for hydrolytic dehydrogenation of AB was developed in this work. Waste-biomass-derived activated carbon was proved to be an excellent material for supporting nanocatalysts. With respect to the bimetal phosphide, the catalytic activity is significantly determined by the ratio of different metal elements, and $Co_{0.8}Cu_{0.2}P$ nanocatalyst supported on the activated carbon presents the optimal activity for AB hydrolysis due to the synergistic effect. Additionally, magnetic feature of the catalyst endows easy separation and reusing, especially in practical applications.

Author contributions

Lei Wei: conceptualization, writing – original draft, writing – review & editing. Yanhong Lu: methodology, supervision. Ruixuan Lu: investigation, formal analysis. Yuxin Cui: investigation, formal analysis.

Conflicts of interest

There are no conflicts to declare.

Acknowledgements

We acknowledge the Natural Science Foundation of Hebei Province, China (E2020408004), Fundamental Research Funds for the Universities in Hebei Province, China (JYQ202002), Research Project of Hebei Education Department, China (ZD2022035), and Innovation Training Project for College Students in Hebei Province, China (S202210100006).

References

1 S. Akbayrak and S. Özkar, *Int. J. Hydrogen Energy*, 2018, **43**, 18592–18606.
2 U. B. Demirci, *Int. J. Hydrogen Energy*, 2017, **42**, 9978–10013.
3 M. Yadav and Q. Xu, *Energy Environ. Sci.*, 2012, **5**, 9698–9725.
4 C. Y. Alpaydin, S. K. Gulbay and C. O. Colpan, *Int. J. Hydrogen Energy*, 2020, **45**, 3414–3434.
5 H. L. Jiang and Q. Xu, *Catal. Today*, 2011, **170**, 56–63.
6 C. Tang, F. Qu, A. M. Asiri, Y. Luo and X. Sun, *Inorg. Chem. Front.*, 2017, **4**, 659–662.
7 C. Y. Peng, L. Kang, S. Cao, Y. Chen, Z. S. Lin and W. F. Fu, *Angew. Chem., Int. Ed.*, 2015, **54**, 15725–15729.
8 J. Yang, Q. Yuan, Y. Liu, X. Huang, Y. Qiao, J. Lu and C. Song, *Inorg. Chem. Front.*, 2019, **6**, 1189–1194.
9 X. Zhou, X. F. Meng, J. M. Wang, N. Z. Shang, T. Feng, Z. Y. Gao, H. X. Zhang, X. L. Ding, S. T. Gao, C. Feng and C. Wang, *Int. J. Hydrogen Energy*, 2019, **44**, 4764–4770.
10 S. H. Li, X. R. Song, Y. T. Li, Y. Q. Zhao and X. C. Zheng, *Int. J. Hydrogen Energy*, 2021, **46**, 27555–27566.
11 M. Yuan, Z. Cui, J. Yang, X. Cui, M. Tian, D. Xu, J. Ma and Z. Dong, *Int. J. Hydrogen Energy*, 2017, **42**, 29244–29253.
12 G. X. Tang, L. Q. Zhang, X. F. Zhu and X. F. Zhu, *Carbon*, 2020, **158**, 930–931.
13 S. Yang, S. Wang, X. Liu and L. Li, *Carbon*, 2019, **147**, 540–549.
14 K. Li, S. Tian, J. Jiang, J. Wang, X. Chen and F. Yan, *J. Mater. Chem. A*, 2016, **4**, 5223–5234.
15 Y. Lu, S. Zhang, J. Yin, C. Bai, J. Zhang, Y. Li, Y. Yang, Z. Ge, M. Zhang, L. Wei, M. Ma, Y. Ma and Y. Chen, *Carbon*, 2017, **124**, 64–71.
16 Y. Li, G. Yang, L. Wei, J. Liu, Y. Zhang, Y. Cui and Y. Zhou, *New J. Chem.*, 2022, **46**, 8256–8262.
17 T. Liu, K. Wang, G. Du, A. M. Asiri and X. Sun, *J. Mater. Chem. A*, 2016, **4**, 13053–13057.
18 A. C. Ferrari and J. Robertson, *Phys. Rev. B: Condens. Matter Mater. Phys.*, 2000, **61**, 14095–14107.
19 X. Hu, X. Sun, S. J. Yoo, B. Evanko, F. Fan, S. Cai, C. Zheng, W. Hu and G. D. Stucky, *Nano Energy*, 2019, **56**, 828–839.
20 Q. Yao, Z. H. Lu, Y. Wang, X. Chen and G. Feng, *J. Phys. Chem. C*, 2015, **119**, 14167–14174.
21 K. Guo, Y. Ding, J. Luo, M. Gu and Z. Yu, *ACS Appl. Energy Mater.*, 2019, **2**, 5851–5861.
22 Q. Liu, S. Zhang, J. Liao, K. Feng, Y. Zheng, B. G. Pollet and H. Li, *J. Power Sources*, 2017, **355**, 191–198.
23 A. Bulut, M. Yurderi, I. E. Ertas, M. Celebi, M. Kaya and M. Zahmakiran, *Appl. Catal., B*, 2016, **180**, 121–129.
24 J. Li, Q. L. Zhu and Q. Xu, *Catal. Sci. Technol.*, 2015, **5**, 525–530.
25 W. Feng, L. Yang, N. Cao, C. Du, H. Dai, W. Luo and G. Cheng, *Int. J. Hydrogen Energy*, 2014, **39**, 3371–3380.
26 X. Wang, J. Liao, H. Li, H. Wang and R. Wang, *J. Colloid Interface Sci.*, 2016, **475**, 149–153.
27 L. Yang, N. Cao, C. Du, H. Dai, K. Hu, W. Luo and G. Cheng, *Mater. Lett.*, 2014, **115**, 113–116.
28 S. Demirci and N. Sahiner, *Fuel Process. Technol.*, 2014, **127**, 88–96.
29 X. Y. Meng, L. Yang, N. Cao, C. Du, K. Hu, J. Su, W. Luo and G. Cheng, *ChemPlusChem*, 2014, **79**, 325–332.
30 N. Sahiner and S. Sagbas, *J. Power Sources*, 2014, **246**, 55–62.
31 Y. Yamada, K. Yano and Q. Xu, *J. Phys. Chem. C*, 2010, **114**, 16456–16462.
32 M. Rakap and S. Özkar, *Catal. Today*, 2012, **183**, 17–25.
33 Y. Yuan, X. Chen, X. Zhang, Z. Wang and R. Yu, *Inorg. Chem. Front.*, 2020, **7**, 2043–2049.
34 L. Wei, X. L. Dong, Y. M. Yang, Q. Y. Shi, Y. H. Lu, H. Y. Liu, Y. N. Yu, M. H. Zhang and Q. Wang, *Int. J. Hydrogen Energy*, 2020, **45**, 10745–10753.
35 X. J. Yang, C. Y. Wang, R. Y. Gao, Z. M. Lu, X. H. Zhang, X. F. Yu and L. L. Li, *Int. J. Hydrogen Energy*, 2018, **43**, 16556–16565.
36 K. Qi, W. Lv, I. Khan and S. Y. Liu, *Chin. J. Catal.*, 2020, **41**, 114–121.
37 Y. Wang, G. Shen, Y. Zhang, L. Pan, X. Zhang and J. J. Zou, *Appl. Catal., B*, 2020, **260**, 118183.
38 Z. Li, t. He, L. Liu, W. Chen, M. Zhang, G. Wu and P. Chen, *Chem. Sci.*, 2017, **8**, 781–788.
39 K. Feng, J. Zhong, B. Zhao, H. Zhang, L. Xu, X. Sun and S. T. Lee, *Angew. Chem., Int. Ed.*, 2016, **55**, 11950–11954.
40 Y. Men, J. Su, X. Du, L. Liang, G. Cheng and W. Luo, *J. Alloys Compd.*, 2018, **735**, 1271–1276.
41 J. Mana, S. Akbayrak and S. Özkar, *RSC Adv.*, 2016, **6**, 102035–102042.
42 C. W. Tsai, H. M. Chen, R. S. Liu, J. F. Lee, S. M. Chang and B. J. Weng, *Int. J. Hydrogen Energy*, 2012, **37**, 3338–3343.
43 L. Wei, Y. Zhang, J. Liu, Y. Li, Y. Lu and Y. Liu, *New J. Chem.*, 2022, **46**, 19731–19739.
44 L. Wei, Q. Liu, S. Liu and X. Liu, *Funct. Mater. Lett.*, 2020, **13**, 1950093.